Solar Energy 269 (2024) 112357

Contents lists available at ScienceDirect

Solar Energy

journal homepage: www.elsevier.com/locate/solener

Nonlinear and multivariate regression models of current and voltage at maximum power point of bifacial photovoltaic strings

Gaetano Mannino [a], Giuseppe Marco Tina [a,*], Gabino Jiménez-Castillo [b], Mario Cacciato [a], Fabrizio Bizzarri [c], Andrea Canino [c]

[a] DIEEI, University of Catania, 95125 Catania, Italy
[b] Department of Electrical Engineering, Center for Advanced Studies in Earth Sciences, Energy and Environment, University of Jaen, Jaen, Spain
[c] Enel Green Power SpA, Viale Regina Margherita, 125, 00198 Rome, Italy

ARTICLE INFO

Keywords:
Bifacial
Monofacial
Photovoltaics
Bifacial modelling
PV monitoring
Photovoltaic models

ABSTRACT

The bifacial photovoltaic (PV) modules are able to convert the irradiance that hits both the front and the back side of the modules into electrical energy, this allows to increase the output power compared to monofacial modules. However, the mathematical models used for traditional PV modules do not consider the contribution of rear irradiance, even recent works deal with the modeling of the rear irradiance influence on bPV power output. In the present work some empirical models capable of estimating the current and voltage at maximum power point conditions are unveiled; the models consider only the front irradiance, as monofacial PV modules, or the back irradiance through the concept of equivalent irradiance and module temperature. In addition, some modifications to the current and voltage models have been proposed. In all cases, the optimal parameters of the models are obtained starting from a dataset of experimental data acquired from a string of bifacial photovoltaic modules installed in Catania (Italy). The PV plant under study was monitored for an entire year, thus allowing the use of data acquired in different weather conditions.

The method description includes the filtering of the input signals and the searching method of the empirical coefficients in order to estimate the current and voltage at the maximum power point (MPP) for bifacial photovoltaic modules.

1. Introduction

Solar energy represents a fundamental resource for the global energy transition towards renewable sources. Photovoltaic (PV) technology is one of the most widely used method for converting solar energy into electrical energy. Traditional monofacial PV (mPV) modules have always dominated the market; however, in recent years, bifacial PV (bPV) modules have become increasingly popular, as they are able to convert the irradiation that hits the modules on both the front and back.

Bifacial modules can generate electrical power from light entering both the front and rear sides, with the bifaciality factor typically ranging from 65 % to 95 % [32]. The rapid advancements in bifacial PV technologies, including cell designs, module innovations, system designs, and performance modeling, are driving the increasing adoption and optimization of bifacial PV systems in the global market [33]. However, the output gain from a bifacial module compared to a monofacial module also depends on external factors such as module orientation and tilt angle, ground albedo, module elevation, height, diffuse irradiance fraction, and self-shading, which affect the angular distribution of light reaching the rear side. Bifacial modules are increasingly used in utility-scale plants with single-axis tracking, providing a broader range of competitive tracking PV plants [2], even if the capability of the modules to convert the rear irradiance allow to increase the production of energy also for fixed tilt PV systems. The report "IRENA Power Generation Costs 2020" [15] provides an overview of the costs of producing electricity from various renewable sources, including bifacial solar modules.

The report [17] provides information on the advancements in photovoltaics, covering aspects such as the materials used, production processes, and the evolution of PV cells, modules, and systems. The increased use of bifacial modules has therefore accentuated the importance of verifying whether the electrical and thermal models developed for monofacial modules are able to describe the behaviour also for bifacial modules.

A PV model is a set of mathematical equations that describes the behaviour of PV cells, modules or strings under different operating

* Corresponding author.
E-mail address: giuseppe.tina@unict.it (G.M. Tina).

https://doi.org/10.1016/j.solener.2024.112357
Received 16 May 2023; Received in revised form 16 December 2023; Accepted 15 January 2024
Available online 28 January 2024
0038-092X/© 2024 The Author(s). Published by Elsevier Ltd on behalf of International Solar Energy Society. This is an open access article under the CC BY license (http://creativecommons.org/licenses/by/4.0/).

Nomenclature

$G_{f,POA}$	Front plane of array irradiance [W/m^2]
$G_{r,POA}$	Rear plane of array irradiance [W/m^2]
$G_{eq,POA}$	Equivalent measured irradiance considering both global front in-plane irradiance ($G_{f,POA}$) and rear in-plane irradiance ($G_{r,POA}$) [W/m^2]
G_0	Irradiance at STC [W/m^2]
I_{mp}	MPP current [A]
$I_{mp,0}$	MPP current at standard test condition [A]
I_{sc}	Short circuit current [A]
P_0	Power at STC [W]
P_{dc}	DC MPP power output [W]
PR	Performance Ratio
T_c	PV cell temperature [°C]
T_m	PV module temperature [°C]
$T_{c,0}$	Temperature at STC [°C]
V_{mp}	MPP voltage [V]
$V_{mp,0}$	MPP voltage at STC [V]
V_{oc}	Open circuit voltage [V]
α_{mp}	Temperature correction coefficients of MPP current [1/°C]
β	temperature coefficient for open circuit Voltage [1/°C]
φ	Bifacial factor
η	Module efficiency

Abbreviations

STC	standard test conditions
MPP	maximum power point
mPV	monofacial photovoltaics
bPV	bifacial photovoltaics

conditions. These models are important tools for monitoring and predicting the performance and optimizing the design parameters of PV plants.

Plane of array irradiance, and cell temperature are important variables to consider in mPV models, whereas for bPV also the rear irradiance needs to be taken into consideration. If the temperature is not directly measured is possible to estimate given the technology of the PV module and the environmental variables such as ambient temperature, irradiance and wind speed. Rear irradiance is influenced by the albedo, mounting structure and height from the ground of the PV modules.

In the literature, it is possible to find a variety of electrical and thermal models for the performance of mPV modules and methods for calculating the required parameters [10]. The model to be chosen should be a compromise between accuracy and simplicity [39,40], also the PV technology can be a criterion for choosing one or the other model [39]. Such models with suitable modifications are also applied to bifacial systems [28].

However, the majority of the works in literature about modelling of bPVs are based on a limited amount of experimental data for optimization and validation of the models. Therefore, the objective of this work is to analyse and validate experimental models of mPV and propose new adaptations for bPV. For this purpose, the experimental parameters of the adopted models were obtained in MATLAB environment.

Regarding of PV models, several types could be applied to estimate the output variables of photovoltaic modules. Analytical methods [25], empirical approaches [31] and recently, machine learning techniques [38,9], have been developed to determine the output power of mPV systems using measured inputs and manufacturers' parameters.

Analytical models are used to estimate the current–voltage and power-voltage curves under operating conditions, using as inputs the cell temperature, irradiance on the plane of the module and parameters from the manufacturer's datasheet [40,20,1,3,6,7,16,26,29,37,41].

The Sandia model, also known as the model defined by King et al., is an example of an empirical model that estimates the electrical output using inputs such as irradiance, cell temperature and empirical coefficients [21].

The availability of models and, in turn, simulation results of bifacial PV modules is an essential factor in promoting the widespread adoption of this technology.

The fundamental differences between mPV and bPV systems, such as the influence of albedo and shading on energy yield, require the development of new and improved models to accurately predict bPV performance [3]. In the review study about bifacial PV technology [12] some of the best-known PV models are reported, including proposed modifications to take in to account the rear irradiance that hits the back side of the modules [11].

The study [42] addresses the development of the energy rating for bifacial modules, also a procedure for the calculation of the rear irradiance is shown.

Another simple electrical performance model was formulated for calculating the short circuit current and open circuit voltage under operating conditions, which were calculated with a linear approximation of standard condition values.

The maximum power point was calculated through Osterwald's correlation. Energy losses were estimated using experiences found in the literature [19]. Another maximum power model was proposed, where only the front and rear illumination of the solar module and the electricity efficiencies of the front and rear PV modules were taken into account [34]. Similarly, a maximum power model for estimating the output power and a NOCT model for estimating the module temperature of a bifacial PV system were proposed, taking into account the front irradiance and the bifacial irradiance ratio. Furthermore, a new bifacial performance ratio was defined [22]. An adaptation of both the analytical one-diode model defined by Eduardo et al. and the empirical model defined by King et al. was proposed to estimate the power output. The results showed that the distribution of the daily errors was better for the analytical model for bifacial modules, with relative errors lower than 4 % [3]. A simplification of the one-diode model was proposed for estimating the maximum power point, short circuit current, open circuit voltage, and efficiency and fill factors using standard indoor measurements on mPV modules [30]. Other authors have used the five-parameter photovoltaic monofacial electrical model directly without any modification in the mathematical expressions [13]. In [18] the measured and estimated maximum power were compared, and the root mean square of 0.15 % differences at STC. The dual monofacial circuit is simulated as both sides are independent, and the effect of the cell side, whether front or back, is neglected [27].

In the present work some empirical correlations capable of estimating the current and voltage at maximum power point (MPP) conditions, considering only the irradiance on the front as in the monofacial case and considering the irradiance on the back through the concept of equivalent irradiance are presented. Some modifications to the existing current and voltage at MPP models have been proposed.

In both cases, the optimal parameters of the models are obtained starting from a dataset of experimental data acquired from a string of bifacial photovoltaic modules installed in Catania (Italy). The PV plant under study was monitored for an entire year, thus allowing the use of data acquired in different weather conditions. Different technologies are used in bPV modules, but the most commonly used cells for bifacial modules are PERC, topCON and HJT cells. In this study, modules with cells made of monocrystalline silicon PERC are used. However, the theoretical aspects presented can also be applied to other bifacial technologies.

The empirical models adopted in this study can be used to generate power at the Maximum Power Point, but also allows the inverter algorithms to be programmed to modulate the power supplied by the photovoltaic strings in off-design conditions if needed.

The PV system, the measurement setup and the description of the data are presented in section 2. The methodology is presented in section 3. Then, in section 4, the results obtained with different models are presented. Finally, the conclusions are drawn in section 5.

2. PV system and data description

The photovoltaic system being studied (Fig. 1 and Fig. 2) is located in Catania at the Enel Innovation Hub & Lab (37.4°,15°). An outdoor area is dedicated to the monitoring of bifacial systems including the photovoltaic system under study. The PV system consists of 7 PV modules, which are connected in series and made up of PERC monocrystalline silicon cells. The modules highlighted in the figure are connected in series and are part of a single string, while the other modules on the same structure belong to a different string and are not monitored in this study. The lower edge of the system is 1080 mm from the ground, while the upper one 2800 mm from the ground. The upper edge of the monitored bifacial modules of the highest monitored string is 2300 mm from the ground. The inclination of the modules is 37.5°. The PV system is located adjacent to another PV system that is placed at 2600 mm. The data was acquired during one-year period from 01/06/2021 to 31/05/2022. The electrical data was acquired by DC voltage and DC current transducers. The plane of array irradiance on the front of the module was measured using a class A pyranometer, while the irradiance on the back of the modules was measured using a reference cell. It is placed 4700 mm from the right side of the system and 2800 mm from the left side of the system, in front view, and it is placed at a height of 1740 mm from the ground.

The module temperature, T_m, is acquired through a PT100 sensor positioned on the back of a module, while the ambient temperature via a thermohygrometer. Wind speed is measured using a cup anemometer placed at a height of 10 m. The ambient temperature, T_{amb} was measured until 10/30/2021 using a thermo-hygrometer located at the same place as the PV plant. Starting from 10/31/2021, a thermo-hygrometer located 300 m away from the plant and close to the anemometric tower was used. The sampling interval is one minute for all data, except for the wind speed data and for the second part of the ambient temperature which have a sampling interval of 10 min. The latter has been readjusted to 1 min by linear interpolation.

3. Data filtering

The data has been filtered to use only data that is meaningful for the analysis. Initially, in Fig. 3, the flowchart of the filtering process is presented, with detailed explanations of each step provided below. The individual variables were filtered, followed by the application of the PR filter, which selectively removed pairs of values where Irradiance and Power were determined to be uncorrelated.

3.1. Irradiance

The threshold values for Irradiance were chosen according to the IEC 61724-1:2021 standard [14]. Even in the standard the minimum irradiance threshold is set to 20 W/m^2, it has been increased to 50 W/m^2 because, for lower irradiance values, numerous outliers could be

Fig. 1. PV system, front view.

Fig. 2. Back view of the bifacial PV modules, reference cell and pt 100, [23].

generated for the electrical quantities. The upper irradiance threshold has been set to 1200 W/m^2, as in the standard.

3.2. Voltage

The voltage and current data must be filtered according to both the characteristics of the modules and the range allowed by the inverter.

The minimum allowable output voltage from the modules was calculated using the formula:

$$V_{lowerlim} = n_{modules} \bullet V_{mp}^{NOMT} \bullet \left[1 - \beta\left(T_{m,max} - T_0\right)\right] \quad (1)$$

Where:

$n_{modules}$ is the number of modules in series, V_{mp}^{NOMT} is the maximum power point Voltage at nominal operating module temperature conditions by the datasheet, β is the thermal coefficient for V_{oc}, $T_{m,max}$ is the maximum module temperature and T_0 is the standard test condition temperature (25 °C).

Maximum recorded temperature recorded by the data for one year is 66.7 °C, but 75 °C has been selected as $T_{m,max}$. The thermal coefficient for V_{mp} is not provided by the datasheet, so the thermal coefficient for V_{oc} is used. Using the Eq. (1) the value of 223.58 V was obtained; however, 250 V has been set as the minimum voltage value. In any case they exceed the minimum operating voltage of the inverter which is equal to 100 V.

The maximum allowable voltage, considering the modules, is given by the formula:

$$V_{upperlim} = n_{modules} \bullet V_{oc}^{STC} \bullet \left[1 - \beta\left(T_{m,min} - T_0\right)\right] \quad (2)$$

Where:

V_{oc}^{STC} is the open-circuit voltage at standard test conditions provided

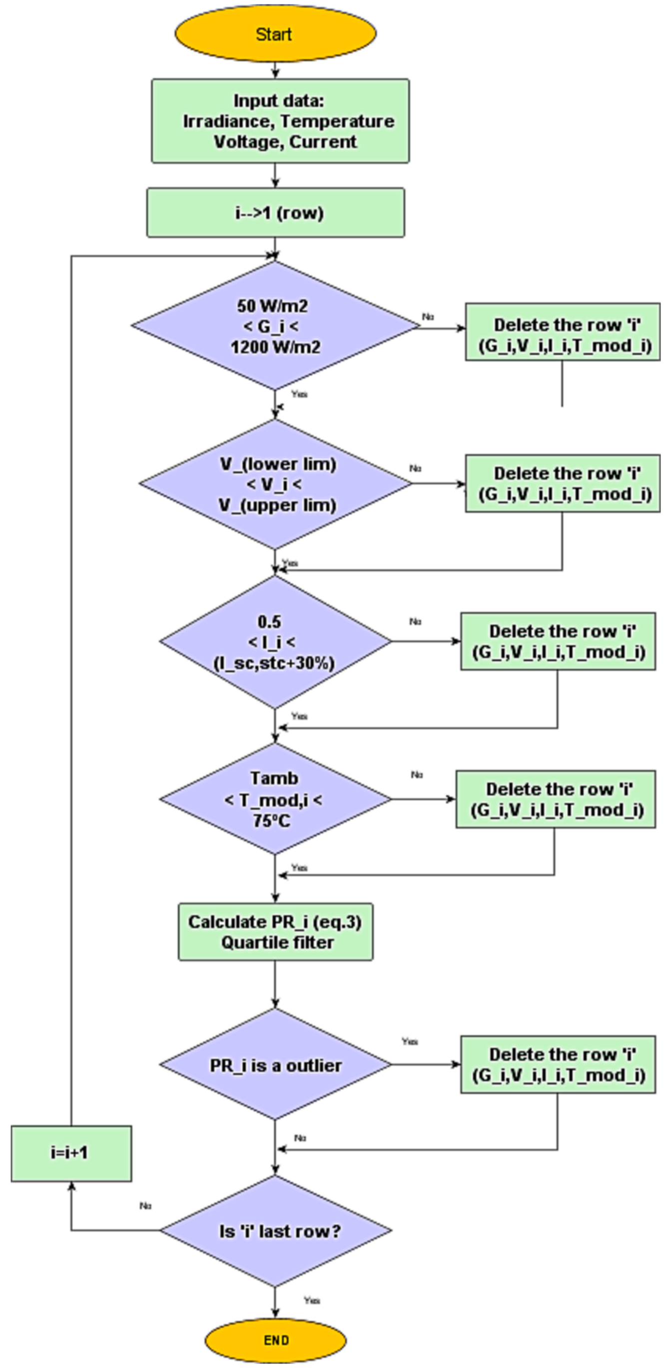

Fig. 3. Filtering flowchart.

by the datasheet, $T_{m,min}$ is the minimum measured module temperature. Is possible to set the recorded minimum module temperature by the dataset. In any case it is necessary to verify that $V_{upperlim}$ is lower than the maximum operating voltage of the inverter, in the case study equal to 500 V. Fig. 4 and Fig. 5 show the voltage before and after applying the filter.

3.3. Current

To filter the current data, the minimum threshold value has been set equal to 0.5 A, while the maximum threshold value has been set equal to the short-circuit current at standard test conditions (STC) from the datasheet; the short circuit current for the bifacial modules of the analysed PV system, in the case of bifacial gain equal to 30 %, correspond to

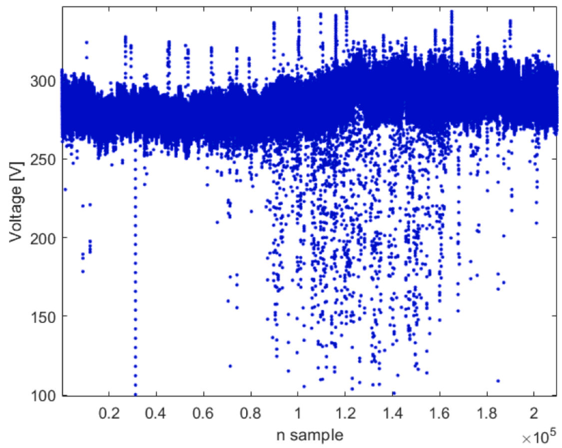

Fig. 4. Unfiltered voltage [V] over one year.

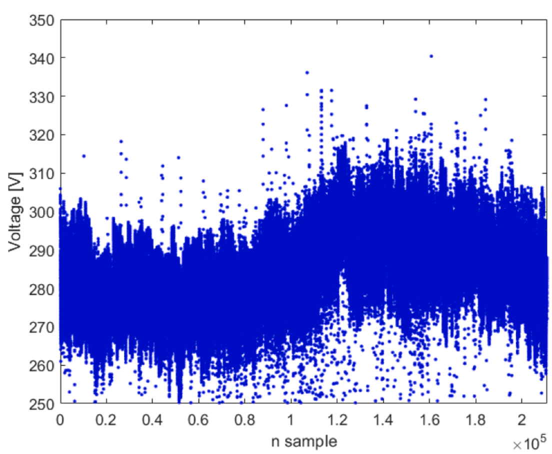

Fig. 5. Filtered voltage [V] over one year.

14 A, approximating by excess. The maximum current threshold value must be lower than the maximum inverter input current, which in the case study is equal to 15 A.

3.4. Temperature

The data has been filtered considering only the samples where the module temperature is greater than or equal to the ambient temperature and where the module temperature is lower than 75 °C.

3.5. Performance ratio

Then the PR filter has been applied to eliminate data where electrical and irradiance values are not correlated. This is typically observed during abrupt transient events or shading conditions that result in electrical output values that are not adequately correlated to the corresponding Irradiance values. The PR is a metric defined as:

$$PR = \frac{\frac{P_{dc}}{P_0}}{\frac{G_{f,POA}}{G_{stc}}} \tag{3}$$

Where P_{dc} is the measured DC Power [W]and P_0 is the Power at STC [W], $G_{f,POA}$ is the front plane of array Irradiance [W/m^2] and G_0 is the Irradiance at STC (1000 W/m^2). Fig. 6 shows the PR values one year, after the application of the previous filters, and the application of the PR filter. The filtering was applied using a filter with a large threshold factor in order to include PR values lower and higher than those characteristic of the system (for example at the beginning and end of the day).

4. Methodology

4.1. Models

Before the models relating to the photovoltaic system, it is necessary to introduce how the irradiance captured by the photovoltaic modules is treated because, together with the operating temperature of the PV modules, it represents the most important parameter. The irradiance captured by the plane of the modules depends on various factors including: position of the sun, atmospheric conditions, and reflectivity of the ground.

In the case of bifacial photovoltaic modules, in addition to the irradiance that hits the front of the modules, it is also useful to consider the irradiance that hits the back of the modules, called rear irradiance.

The horizontal albedo ρ_H is the proportion of the incident light reflected by a ground surface as measured in a horizontal plane.

The in-plane rear-side irradiance ratio ρ_i is the ratio of the incident irradiance on the rear side of the PV array modules to the irradiance incident on the front side

$$\rho_i = \frac{G_{r,POA}}{G_{f,POA}} \tag{4}$$

The in-plane rear-side irradiance ratio ρ_i is similar to the albedo but refers to the plane of the modules, while the albedo refers to the horizontal plane.

$G_{eq,POA}$ is the equivalent irradiance that takes into account both global front in-plane irradiance ($G_{f,POA}$) and rear in-plane irradiance ($G_{r,POA}$) and for bifacial module it can be calculated as:

$$G_{eq,POA} = G_{f,POA} + \varphi \bullet G_{r,POA} \tag{5}$$

Where β is the bifaciality factor.

4.2. Sandia model

The equations and applications associated with the photovoltaic array performance model developed at Sandia National Laboratories are widely described in [21], considering exclusively the current and voltage in the maximum power point conditions, they are represented as follows:

$$I_{mp} = I_{mp,0} \bullet \left(C_0 \bullet G_{f,POA} + C_1 \bullet G_{f,POA}^2\right) \bullet \left(1 + \alpha_{mp} \bullet \left(T_c - T_{c,0}\right)\right) \tag{6}$$

Where $I_{mp,0}$ is the maximum power point current at standard test condition (STC), as reported in the datasheet, $G_{f,POA}$ is the frontal plane of array irradiance, α_{mp} is the thermal coefficient for I_{mp}. T_c is the cell temperature and $T_{c,0}$ is the standard test condition temperature (25 °C). C_0 and C_1 are empirical coefficients.

$$V_{mp} = V_{mp,0} \bullet (1 + \sigma_{mp} \bullet \left(T_c - T_{c,0}\right) + \delta_1 \bullet \ln\left(\frac{G_{f,POA}}{G_0}\right) + \delta_2 \bullet \ln^2\left(\frac{G_{f,POA}}{G_0}\right) \tag{7}$$

Where σ_{mp}, $\delta_1 and \delta_2$ are correction coefficients depending on the module, $V_{mp,0}$ is the maximum power point voltage at standard test conditions (STC), $T_{c,0}$ is cell temperature at STC and $G_{f,POA}$ is global front in-plane irradiance.

4.3. Cristaldi model

In a recent study on the application of a model-based algorithm for power control strategy of photovoltaic modules [5], simplified equations are used compared to those of the Sandia model, but which preserve a similar form. In [5] the maximum power point current is given

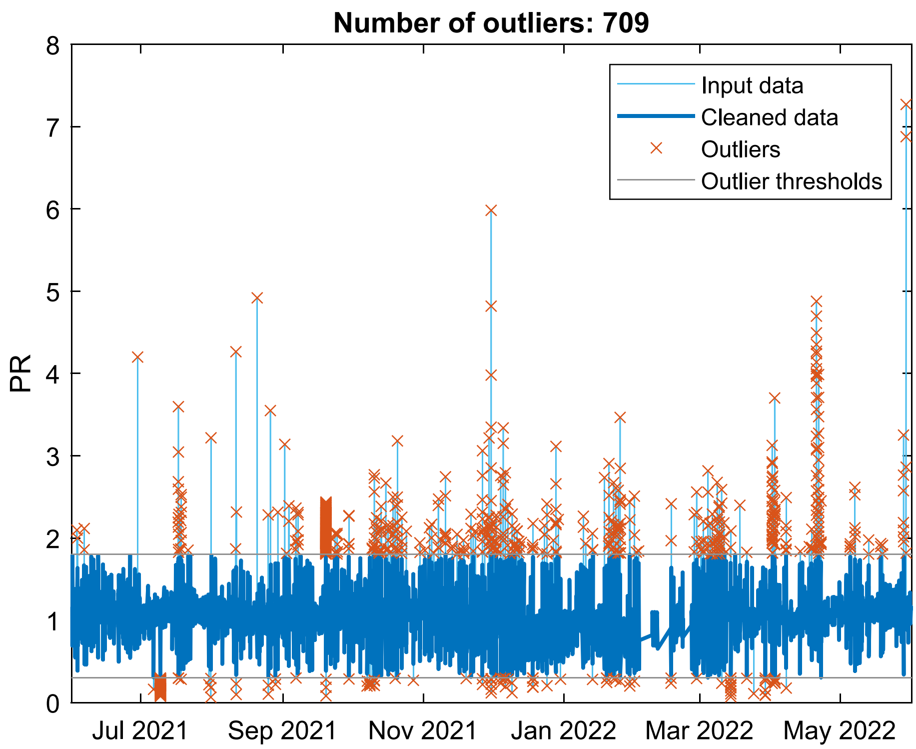

Fig. 6. PR filter, it is used to remove data where DC power and irradiance are not correlated.

by:

$$I_{mp} = I_{mp,0} \bullet \left(\frac{G_{f,POA}}{G_0}\right) \bullet \left(1 + \alpha_{mp} \bullet \left(T_c - T_{c,0}\right)\right) \tag{8}$$

Where α_{mp} is the temperature correction coefficients of MPP current.

In [8] the Eq. (7) of maximum power point voltage has been rearranged in the following four parameters equation:

$$V_{mp} \approx A_0 + A_1 \bullet T_c + A_2 \bullet \ln\left(\frac{I_{mp}}{I_{mp,0}}\right) + A_3 \bullet \ln^2\left(\frac{I_{mp}}{I_{mp,0}}\right) \tag{9}$$

The ratio of currents inside the logarithm can assume values greater or smaller than one this means that the log can assume negative or positive values, this could have an impact on the evaluation of the coefficients so also a non-normalized form of (9) has been considered, in [5] and [4] it is rewritten as follows:

$$V_{mp} \approx A_0 + A_1 \bullet T_c + A_2 \bullet \ln\left(I_{mp}\right) + A_3 \bullet \ln^2\left(I_{mp}\right) \tag{10}$$

5. Method

The aim of this study is to use simple models for voltage and current estimation under maximum power point conditions, I_{mp} and V_{mp}, in the case of bifacial photovoltaic modules. To obtain the empirical coefficients of the considered models, it is possible to use the experimental datasets acquired from a PV system equipped with bifacial modules, such datasets are made by environmental and operative electrical and thermal quantities. The tuned models will allow to obtain the values of I_{mp} and V_{mp} given some relevant measured quantities, such as: irradiance and module temperature.

As a first step the expression of the adapted models have to be defined as explained in the following.

Regarding the evaluation of I_{mp}, the Eqs. (6) and (8) have been modified in order to consider also the back irradiance hitting the modules. The equivalent irradiance has been used as input of the models instead of the frontal irradiance on the plane of the modules. The Eq. (6) and Eq. (8) has been rewritten to adapt it for bifacials, the term $G_{eq,POA}$ has been taken into account as follows:

$$I_{mp} = I_{mp,0} \bullet \left(C_0 \bullet G_{eq,POA} + C_1 \bullet G_{eq,POA}^2\right) \bullet \left(1 + \alpha_{mp} \bullet \left(T_c - T_{c,0}\right)\right) \tag{10}$$

$$I_{mp} = I_{mp,0} \bullet \left(\frac{G_{eq,POA}}{G_0}\right) \bullet \left(1 + \alpha_{mp} \bullet \left(T_c - T_{c,0}\right)\right) \tag{11}$$

About the evaluation of V_{mp}, the Eqs. (9) and (10) have been used:

- Leaving Eqs. (9) and (10) unchanged, using the measured maximum power point current as input.
- By inserting the frontal irradiance on the plane of the modules instead of the current:

$$V_{mp} \approx A_0 + A_1 \bullet T_c + A_2 \bullet \ln\left(\frac{G_{f,POA}}{G_0}\right) + A_3 \bullet \ln^2\left(\frac{G_{f,POA}}{G_0}\right) \tag{12}$$

$$V_{mp} \approx A_0 + A_1 \bullet T_c + A_2 \bullet \ln\left(G_{f,POA}\right) + A_3 \bullet \ln^2\left(G_{f,POA}\right) \tag{14}$$

- By inserting the equivalent irradiance on the plane of the modules instead of the current:

$$V_{mp} \approx A_0 + A_1 \bullet T_c + A_2 \bullet \ln\left(\frac{G_{eq,POA}}{G_0}\right) + A_3 \bullet \ln^2\left(\frac{G_{eq,POA}}{G_0}\right) \tag{13}$$

$$V_{mp} \approx A_0 + A_1 \bullet T_c + A_2 \bullet \ln\left(G_{eq,POA}\right) + A_3 \bullet \ln^2\left(G_{eq,POA}\right) \tag{16}$$

To calculate I_{mp} and V_{mp} for bifacial modules it is possible to use both the monofacial models described in the previous section and the bifacial models described above.

- If monofacial models are used, it is necessary to identify the parameters of the models in correspondence with different albedo values, in this way the back irradiance is indirectly taken into account; therefore, the back irradiance will influence the current and voltage value without being used directly as input to the models. It would therefore be possible to use the coefficients of the calculated models, for the same bifacial modules in the same albedo conditions for which they were obtained.

- If the models for bifacial modules are used, the equivalent irradiance is inserted instead of the front irradiance in monofacial models. That is the actual irradiance that is subjected to electrical conversion (considering efficiency of the modules), however irradiance on the front and on the back do not have a proportional trend, especially at dawn and dusk. Therefore, this option must be carefully weighted and must take into account the positioning of the sensors with respect to the modules.

The models applied to bifacial modules are affected by a greater uncertainty than the models applied to single-facial modules, due to the non-uniformity of the distribution of radiation on the back of the modules, it can vary according to various factors such as the composition of the soil (albedo), the PV mounting structure and other factors. The effect of the albedo and back irradiance for bifacial modules needs to be considered more in detail to obtain a more accurate analysis. Some studies focus on the albedo, such as [43] where a mathematical model to cluster all the influential parameters of the albedo is presented. Therefore, dealing with bifacial modules implies to deal with gain in irradiance received but also with higher uncertainty for the estimation of electrical quantities.

The MATLAB curve fitting toolbox [24] has been used to obtain the optimal empirical coefficients of the I_{mp} and V_{mp} models according to the equations in the designated form. The same toolbox is used in [36] and [35] for the estimation of I_{mp} and V_{mp}. It allows, through the nonlinear least squares method (NLLS), to fit nonlinear models to the data. Nonlinear models are more difficult to fit than linear models because the coefficients cannot be estimated using simple matrix techniques. Instead, an iterative approach is required. The approach for the search of the optimal coefficients used in the present study is the Trust-region method. It must be used for the cases in which the constraints of the coefficients are assigned; however, it has produced satisfactory results even without constraints for the coefficients. Only in 3 out of the 21 cases analysed, for voltage estimation, it has not been possible to find the optimal coefficients with the Trust-region method, therefore the Levenberg-Marquardt algorithm was used, which allowed to find the optimal coefficients also in these cases.

Whether the Trust-region method or the Levenberg-Marquardt method is used, robust regression can be used to minimize the influence of outliers. For each model used in the present study, two robust regression methods were applied:

- Least absolute residuals (LAR): The extreme values have less influence on the fit, since it minimizes the absolute difference of the residuals rather than the squared differences.
- Bisquare weights (Bis): This method minimizes a weighted sum of squares, where the weight given to each data point depends on how far the point is from the fitted line.

Finally, the search for the optimal coefficients for the equations was done using data of a whole year.

6. Results and discussion

6.1. Current models

Two different models have been applied to describe the behaviour of the current: the Sandia model, consisting of two input variables and 3 empirical coefficients, and the Cristaldi model, also consisting of two variables, but only one coefficient. According to the method section both Sandia and Cristaldi models are tested considering two alternatives for the irradiance input: frontal irradiance ($G_{f,POA}$) or Equivalent irradiance (G_{eq}).

The coefficients have been calculated using the experimental filtered dataset by applying three methods: nonlinear least squares method directly (NLLS), Least Absolute Regression (LAR) fitting and Bisquare fitting (Bis). In Table 1 the calculated coefficients and the evaluation of the models though R^2 and RMSE metrics are reported. In Figs. 7–10, the surfaces representing the models and the real points are shown, the residuals are represented in the lower part of the figure for each model. In the appendix A, detailed information about Figs. 7–10 can be found. There is a representation of both the estimated and measured current against module temperature while keeping irradiance constant (400 W/m^2, 600 W/m^2, 800 W/m^2, and 1000 W/m^2). Similarly, the currents are depicted against radiation while maintaining constant module temperature (15 °C, 25 °C, 35 °C, 45 °C, 55 °C). In all 2D graphs, a double y-axis is used, where the right y-axis represents the relative percentage error between measured and estimated values. As observed in the graphs, the majority of the percentage error is below 10 %.

The reported methodology found that the Cristaldi model, despite having a simplified setting of the equation compared to the Sandia model, manages to achieve high accuracy ($R^2 = 0.9761$ in the worst case).

It is possible to observe that to estimate the current using the Sandia model and the Cristaldi model, the use of the equivalent irradiance rather than the irradiance on the plane of the modules (finding the optimal coefficients both in the first and in the second case), has not introduced any significant changes. In principle, therefore, by assigning an albedo value indicative of the site, it would be possible to describe the DC current using models that exclusively use the irradiance on the plane of the modules.

However, the albedo can change seasonally and throughout the day. Furthermore, it must be considered the fact that the use of the equivalent irradiance rather than the irradiance on the plane of the modules may not have introduced significant improvements in the models since the reference cell, that acquires the irradiance on the back of the modules, is located in a specific point of the array and therefore it is not indicative of the irradiance that affects the whole array. The problem of the variability of the irradiance on the back could be investigated by a greater number of sensors able to describe the variability of the irradiance on the back of the modules.

The spectrum of irradiance hitting the modules is another aspect that should be considered. The irradiance that hits the back of the modules will have a spectrum that is different from the one that hits the front of the modules; thus, a different percentage of irradiance could be converted into electrical energy.

For the current, the model that has provided the best results is the Sandia model, however the improvement, if compared to the introduction of two further empirical coefficients, may not justify its use. It should be noted that using the Sandia model, the insertion of the equivalent irradiance rather than the irradiance on the front of the modules produced an improvement, while using the Cristaldi model produced a worsening of the estimate, the differences in the goodness of the model however are mild.

6.2. Voltage model

The V_{mp} varies depending on the environmental conditions such as temperature and solar irradiance. Generally, the V_{mp} increases with increasing solar irradiance, while it decreases with increasing temperature.

In this work the empirical models that has been used to describe the Voltage at maximum power point have the same structure of Eq. (9), according [8], or 10 according [5] and [4] where the I_{mp} is non-normalized respect to standard test conditions (STC).

However, in addition to using the I_{mp} as input, the empirical coefficients of the model were searched using the irradiance or the

Table 1
MPP Current models: coefficients and fitting metrics.

MODEL	INPUT	method	α	C0	C1	R^2	RMSE
Cristaldi	$G_{f,POA}$, T_m (Eq. (8))	NLLS	0.002131			0.9761	0.508
		LAR	0.00215			0.989	0.345
		BIS	0.002192			0.9934	0.2674
	$G_{eq,POA,}$, T_m (Eq. (12)	NLLS	−0.002079			0.9737	0.5322
		LAR	−0.001841			0.9889	0.3453
		BIS	−0.001897			0.9896	0.3349
Sandia	$G_{f,POA}$, T_m (Eq. (6))	NLLS	0.001177	0.001082	−7.247e−08	0.9778	0.4889
		LAR	0.0008604	0.001085	−6.708e−08	0.991	0.3113
		BIS	0.0007338	0.001077	−5.44e−08	0.996	0.2013
	$G_{eq,POA}$, T_m (Eq. (11))	NLLS	0.001242	0.0009288	7.321e−09	0.9797	0.4678
		LAR	0.0008836	0.0009287	1.653e−08	0.9939	0.2567
		BIS	0.0008144	0.0009227	2.456e−0.8	0.9959	0.2114

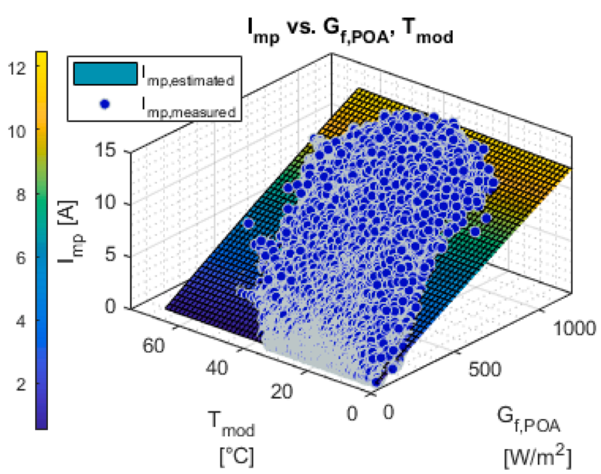

Fig. 7. Sandia model (Eq. (6)), Current vs Front plane of array Irradiance vs Module temperature.

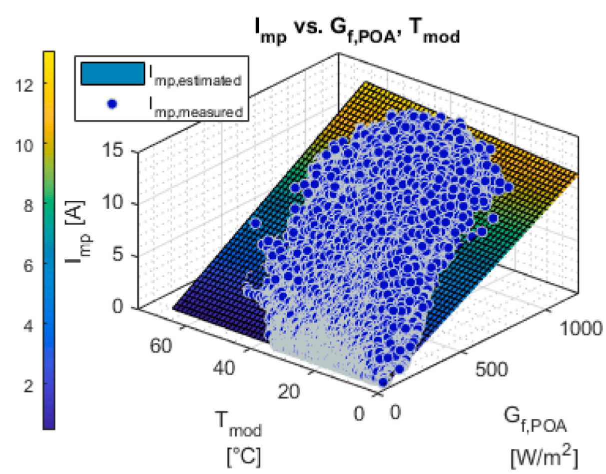

Fig. 9. Cristaldi model (Eq. (8)), Current vs Front plane of array irradiance vs Module temperature.

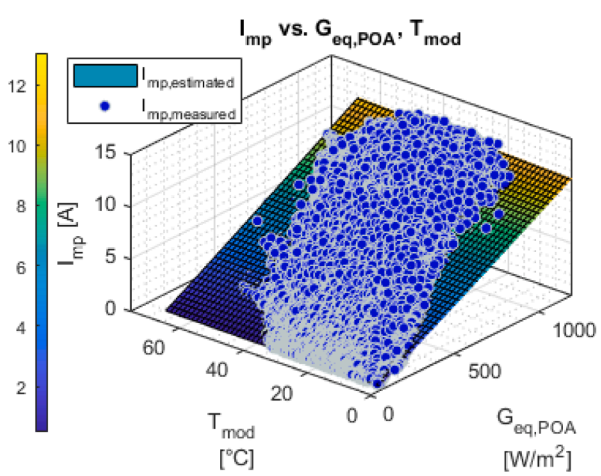

Fig. 8. Sandia model (Eq. (11)), Current vs Equivalent irradiance vs Module temperature.

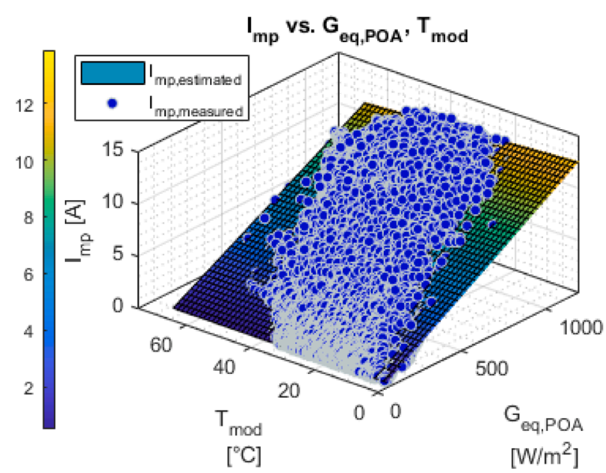

Fig. 10. Cristaldi model (Eq. (12)) Current vs Equivalent irradiance vs Module temperature.

equivalent irradiance instead of the current. This was possible because irradiance and current have an almost linear relationship, while the influence of temperature is already considered within the voltage model. In Table 2 are represented the coefficients obtained for the voltage using the normalized equations (9-13-15) while in Table 3 the results applying the non-normalized form of the same equations (10-14-16).

Figs. 11–13 graphically represent the voltage models through surfaces and the points that represent the experimental values of the dataset. There is a representation of both the estimated and measured voltage against module temperature while keeping irradiance constant (400 W/m^2, 600 W/m^2, 800 W/m^2, and 1000 W/m^2) or current (2.5 A, 5 A, 7.5 A and 10A). Similarly, the currents are depicted against irradiance while maintaining constant module temperature (15 °C, 25 °C, 35 °C, 45 °C, 55 °C). In all 2D graphs, a double y-axis is used, where the right y-

Table 2
MPP Voltage models: coefficients and fitting metrics (normalized input).

MODEL	INPUT	method	A_0	A_1	A_2	A_3	R^2	RMSE
Cristaldi- Faifer	I_{mp}, T_m (Eq. (9))	NLLS	314.7	−0.9275	−3.93	−3.771	0,8159	4.325
		LAR	313.9	−0.9159	−4.48	−4.009	0,8927	3.302
		BIS	313.9	−0.9162	−4.502	−4.022	0,898	3.219
	$G_{f,POA}$, T_m (Eq. (13))	NLLS	314	−0.9204	−4.484	−3.814	0,841	4.019
		LAR	314	−0.9204	−4.484	−3.814	0,841	4.019
		LAR*	314	0.92	−4.499	−3.819	0.8646	3.709
		BIS	314	−0.9204	−4.484	−3.814	0,841	4.019
		BIS*	314	−0.9218	−4.472	−3.812	0.8974	3.229
	$G_{eq,POA}$, T_m (Eq. (15))	NLLS	315.8	−0.9496	−3.456	−4.054	0,8348	4.098
		LAR	314.7	−0.9296	−3.948	−4.167	0,8225	4.246
		BIS	314.8	−0.9318	−3.879	−4.122	0,9032	3.136

* Levenberg-Marquardt algorithm was used to find the optimal coefficients in these cases.

Table 3
MPP Voltage models: coefficients and fitting metrics (non-normalized input).

MODEL	INPUT	method	A_0	A_1	A_2	A_3	R^2	RMSE
Cristaldi- Faifer	I_{mp}, T_m (Eq. (10))	NLLS	303.7	−0.9275	13.43	−3.771	0.8159	4.325
		LAR	303	−0.916	13.98	−4.008	0.8902	3.34
		BIS	303	−0.9162	14.02	−4.022	0.898	3.219
	$G_{f,POA}$, T_m (Eq. (14))	NLLS	169.1	−0.9339	46.14	−3.624	0.8229	4.242
		LAR	163	−0.9205	48.21	−3.814	0.9105	3.015
		BIS	163	−0.9218	48.19	−3.812	0.8974	3.229
	$G_{eq,POA}$, T_m (Eq. (16))	NLLS	146.2	−0.9496	52.55	−4.054	0.8348	4.098
		LAR	143.2	−0.9296	53.62	−4.166	0.8374	4.064
		LAR*	143.1	−0.929	53.63	−4.169	0.8547	3.842
		BIS	144.9	−0.9318	53.07	−4.122	0.9032	3.136

* Levenberg-Marquardt algorithm was used to find the optimal coefficients in these cases.

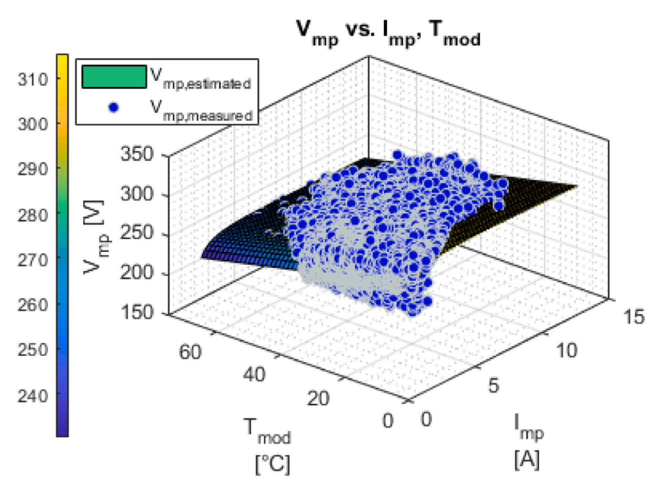

Fig. 11. Cristaldi-Faifer model (Eq. (9)), Voltage vs Current vs Module temperature.

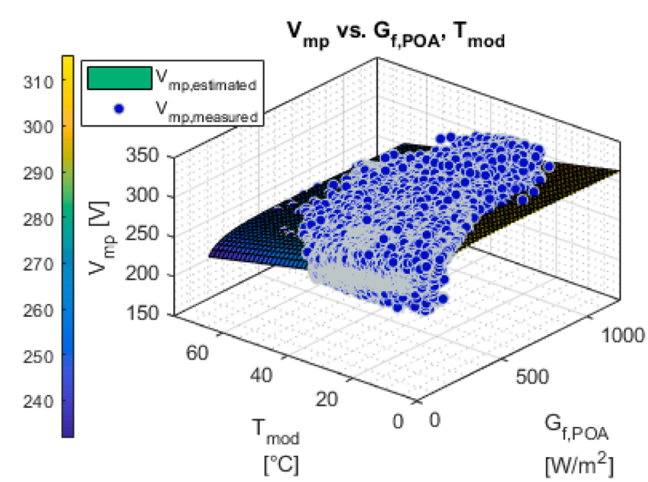

Fig. 12. Cristaldi-Faifer model (Eq. (13)), Voltage vs Front irradiance vs Module temperature.

axis represents the relative percentage error between measured and estimated values. As observed in the graphs, the majority of the percentage error is below 5 % (see Fig. 14).

As expected, the empirical coefficients obtained for the normalized form of the equations using current (9), front irradiance (13), and equivalent irradiance (15) are similar to each other, given the proportionality of current and irradiance.

In the case of NLLS fitting and non-normalized input the model that has given the best results is the one that uses the equivalent irradiance as an input beyond the temperature of the module; followed by the model using the front irradiance and last the model using the current; using the normalized input the best fitting results have been reached using the current, followed by the irradiance while the worse have been reached using equivalent irradiance. Therefore, the normalization of the input quantities is a factor that influences the goodness of fit metrics.

In the case of the LAR fitting, the V_{mp} model, with non-normalized input, that gave the best results is the one that uses the front irradiance as input, followed by the one that uses the current, while the use of the equivalent irradiance gave the worst result; with normalized input the the V_{mp} model using equivalent irradiance as input gave the worse result also, but the use of the current gave better results than using the frontal irradiance.

In the case of Bisquare fitting, the model that has provided the best results uses the equivalent irradiance as input, followed by the one that uses the current and by the one that uses the frontal irradiance, however the differences in the goodness of fit metrics were negligible. Even when normalized inputs are used, the differences in terms of R^2 and RMSE between one case and the other are negligible; non-normalized and normalized input gave similar RMSE and R^2 values.

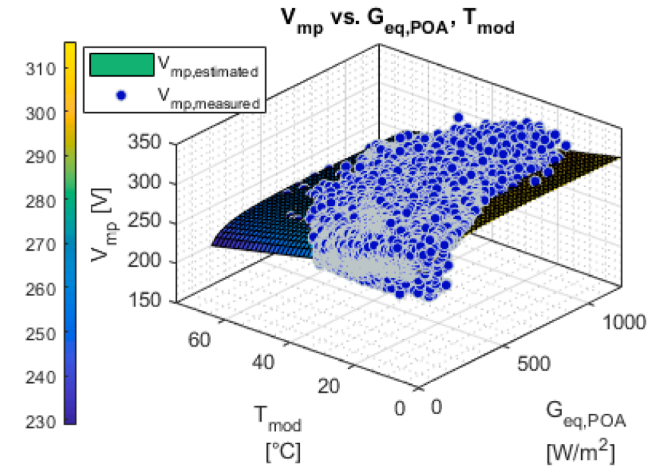

Fig. 13. Cristaldi-Faifer model (Eq. (15)), Voltage vs Equivalent irradiance vs Module temperature.

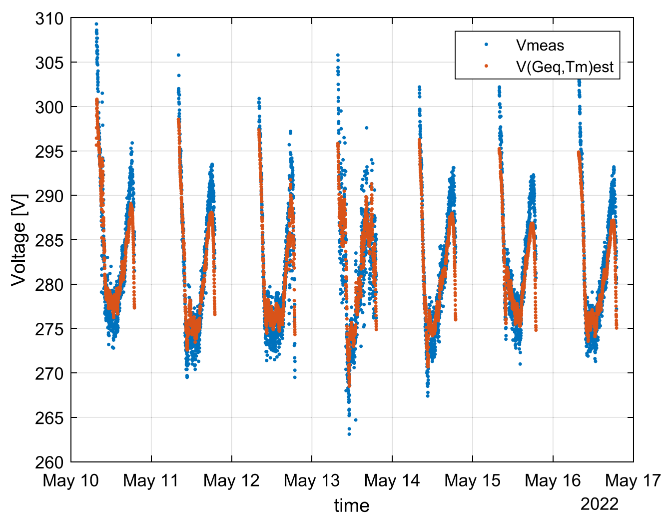

Fig. 14. Measured voltage vs Voltage estimate using Equivalent irradiance and Module temperature as input (Eq. (16)).

The correlations of the voltage at mpp that have the irradiance as an input, have better values of RMSE compared to the case of current as input in both cases (normalized and non-normalized inputs). These results can be justified by the consideration that irradiance and current at mpp are mainly proportional, but the effect of temperature of the PV cell introduce a secondary effect that can be important a low irradiance. Furthermore, the measured current and irradiance data are entered as input of the voltage model; since the sampling time in the case study is one minute, in transient conditions it is possible for one of the two quantities to be recorded before the other, which could influence the voltage estimate.

The figure below shows the weekly trend of the measured voltage and of the voltage estimated in the case of fitting carried out via NLLS and by entering the equivalent irradiance as input (Eq. (16)).

It is possible to see that the estimated values follow the trend of the measured voltage. A deviation between the estimated and measured values can be observed at low levels of irradiance, as can be seen in **figures 16a-16c where the daily trend is zoomed using respectively I, G and G_{eq}.

The measured and estimated voltage curve have the same trend, as shown in the Fig. 15. However, the continuous voltage oscillation caused by the algorithm implemented in the inverter to track the maximum power point results in higher values of RMSE(Root Mean

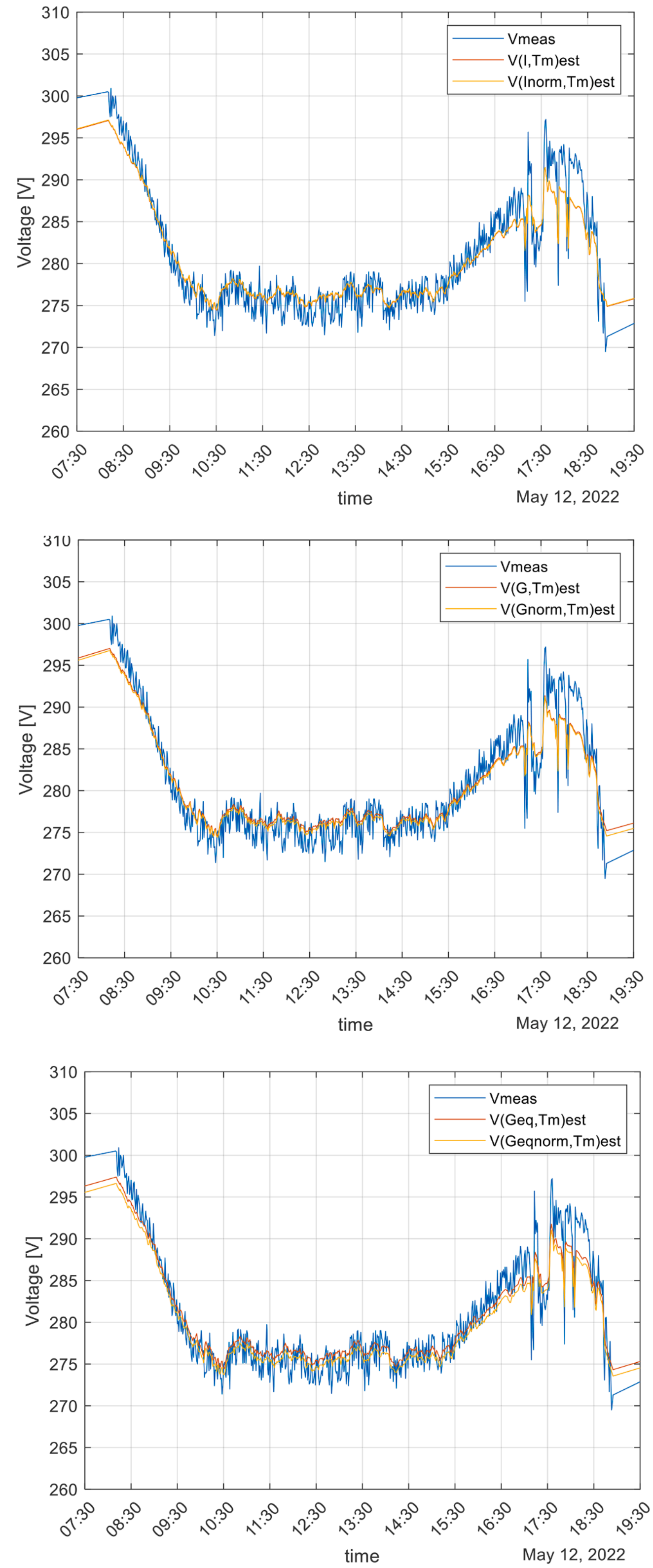

Fig. 15. Voltage measured vs Voltage estimated using different input, From top to down: $V_{mp}(I_{mp},T_m)$ (Eq. (9), Eq. (10)) $V_{mp}(G_{f,POA},T_m)$ (Eq. (13), Eq. (14)) $V_{mp}(G_{eq,POA},T_m)$ (Eq. (15), Eq. (16)).

Square Error).

This suggests that the measured and estimated voltage curves have a similar pattern, but the algorithm implemented in the inverter causes continuous oscillations in the voltage, which results in higher values of

RMSE. The RMSE is a measure of how much the estimated values differ from the measured values. In this case, the higher RMSE indicates that there is a larger difference between the estimated and measured values due to the algorithm's continuous voltage oscillation.

An important aspect of the adopted empirical models is the ability to generalize them for strings with a different number of modules. Assuming uniformity in the operational performance of the modules, it would be possible to obtain the voltage at mpp of a single module as well as string.

Once the empirical model at the string level is obtained, which in the case study is equipped with bifacial modules with PERC monocrystalline silicon cells, it is possible to approximately extend the model by using the following equation:

$$P_{mp,mod} = \frac{P_{mp,string}}{n_{mod}} = \frac{V_{mp,string} \bullet I_{mp,string}}{n_{mod}} \tag{17}$$

By substituting the voltage model instead of $V_{mp,string}$ and assuming that the current of the modules in series is equal to that of a single module, it is possible to obtain:

$$\begin{aligned} &\frac{\left(A_0 + A_1 \bullet T_c + A_2 \bullet \ln(I_{mp}) + A_3 \bullet \ln^2(I_{mp})\right) \bullet I_{mp,string}}{n_{mod}} \\ &= \left[\frac{A_0}{n_{mod}} + \frac{A_1}{n_{mod}} \bullet T_c + \frac{A_2}{n_{mod}} \bullet \ln(I_{mp}) + \frac{A_3}{n_{mod}} \bullet \ln^2(I_{mp})\right] \bullet I_{mp,string} \\ &= V_{mp,mod} \bullet I_{mp,string} \end{aligned} \tag{18}$$

The current of modules in series is not equal to that of a single module, due to losses and different operating voltage, however theoretically it can be approximated with the string current.

By inserting the current, the front irradiance, or the equivalent irradiance as inputs, the trend of the estimated voltage and the measured voltage, even for low irradiance values, reflects the behaviour of the measured voltage.

With the purpose of applying the model in different locations and environmental conditions, it is not a trivial decision to choose whether to use current, front irradiance, or equivalent irradiance as inputs for the voltage model.

If front irradiance is chosen, particularly during sunrise and sunset when the front and back irradiance are not proportional, neglecting the back irradiance can lead to errors in voltage estimation if the model coefficients are obtained under the same conditions as the PV system where it will be applied. However, if the albedo and mounting structure differ from the case study, considering the equivalent irradiance or calculating new model coefficients based on the front irradiance as input becomes necessary.

Since the current is already influenced by both front and back irradiance, the irradiance indirectly affects the voltage model when the current is included as an input.

The models used are all calibrated using I_{mp} and V_{mp}. However, the contributions of back irradiance and front irradiance are not treated separately, as this would result in additional studies being required. Another aspect to consider is that, in order to accurately describe the ideal operating conditions of PV modules, the models should be calibrated after the quality check of the modules themselves following their installation. In this way, damaged cells or "bottleneck" issues in the case of modules connected in series would not affect the output estimation.

7. Conclusion

In this work, we have reported and adapted several empirical models for estimating the current and voltage at the maximum power point of bifacial modules. The models were tested by inserting as input, alongside the module temperature, which is present in all the models used, three alternative variables: current, plane of array frontal irradiance, and equivalent irradiance. The empirical coefficients of the models were calculated based on experimental data from a PV system equipped with bifacial modules, and the measured values were compared with the estimated values from the models to assess their accuracy. The coefficients should be recalculated when considering different system configurations and module technologies. The results show that:

1) It is possible to use irradiance rather than current as an input in the voltage model.
2) As the fitting method varies, the results may change.

There are various ways of correlating the variables with each other, only some of those present in the literature, simple and replicable, have been reported here. However, there are numerous expressions for correlating the variables with each other, and the way of representing this correlation can be different according to the application for which the model is used. Further research will be able to evaluate in a more precise way the effect of irradiance on the back of the modules through advanced distributed sensors.

It was possible to model the current and voltage at the maximum power point, considering the environmental variables such as irradiance on the front and back of the module array, as well as the module temperature. The input signal filtering method and the approach used to determine the empirical coefficients in MATLAB environment were described.

Further studies could verify the effectiveness of using empirical coefficients to derive the voltage profile for individual modules or strings composed of a different number of modules compared to the string analyzed in the present study. It would be also possible to replicate the models for different photovoltaic technologies.

There are multiple approaches to establish correlations among the variables, but this study focuses on reporting the simple and reproducible forms. The empirical models presented in this study can be used for various purposes, including monitoring of PV strings, detection of faulty conditions, soiling effects, or degradation phenomena.

Declaration of competing interest

The authors declare that they have no known competing financial interests or personal relationships that could have appeared to influence the work reported in this paper.

Acknowledgements

This work is supported by Ministero dell'Istruzione, dell'Università e della Ricerca (Italy) (grant PRIN2020-HOTSPHOT 2020LB9TBC).

Appendix A. Supplementary data

Supplementary data to this article can be found online at https://doi.org/10.1016/j.solener.2024.112357.

References

[1] M.N. Akram, S. Lotfifard, Modeling and health monitoring of DC side of photovoltaic array, IEEE Trans. Sustain. Energy 6 (4) (2015) 1245–1253, https://doi.org/10.1109/TSTE.2015.2425791.
[2] Berrian, D., Libal, J., Klenk, M., Nussbaumer, H., & Kopecek, R. (2019). Performance of Bifacial PV Arrays With Fixed Tilt and Horizontal Single-Axis Tracking : Comparison of Simulated and Measured Data. 9(6), 1583–1589.
[3] S. Bouchakour, D. Valencia-caballero, A. Luna, E. Roman, E. Amin, K. Boudjelthia, P. Rodr, Modelling and simulation of bifacial PV production using monofacial electrical models, Energies 14 (4224) (2021) 1–16.
[4] L. Cristaldi, M. Faifer, C. Laurano, R. Ottoboni, S. Toscani, M. Zanoni, Model-based maximum power point tracking for photovoltaic panels: Parameters identification and training database collection, IET Renew. Power Gener. 14 (15) (2020) 2876–2884, https://doi.org/10.1049/iet-rpg.2020.0101.
[5] L. Cristaldi, M. Faifer, C. Laurano, E. Petkovski, S. Toscani, R. Ottoboni, An innovative model-based algorithm for power control strategy of photovoltaic panels, Conference Record - IEEE Instrumentation and Measurement Technology Conference 1–6 (2022), https://doi.org/10.1109/I2MTC48687.2022.9806605.

[6] W. De Soto, S.A. Klein, W.A. Beckman, Improvement and validation of a model for photovoltaic array performance, Sol. Energy 80 (1) (2006) 78–88, https://doi.org/10.1016/j.solener.2005.06.010.
[7] A.A. EL Tayyan, A simple method to extract the parameters of the single-diode model of a PV system, Turk. J. Phys. 37 (1) (2013) 121–131, https://doi.org/10.3906/fiz-1206-4.
[8] Faifer, M., Cristaldi, L., Toscani, S., Soulantiantork, P., & Rossi, M. (2015). Iterative model-based Maximum Power Point Tracker for photovoltaic panels. 2015 IEEE International Instrumentation and Measurement Technology Conference (I2MTC) Proceedings, 1273–1278. https://doi.org/10.1109/I2MTC.2015.7151456.
[9] C. Ghenai, F.F. Ahmad, O. Rejeb, M. Bettayeb, Artificial neural networks for power output forecasting from bifacial solar PV system with enhanced building roof surface Albedo, J. Build. Eng. 56 (June) (2022) 104799, https://doi.org/10.1016/j.jobe.2022.104799.
[10] A. Gholami, M. Ameri, M. Zandi, R. Gavagsaz Ghoachani, Electrical, thermal and optical modeling of photovoltaic systems: Step-by-step guide and comparative review study, Sustainable Energy Technol. Assess. 49 (June 2021) (2022) 101711, https://doi.org/10.1016/j.seta.2021.101711.
[11] A. Gholami, M. Ameri, M. Zandi, R. Gavagsaz Ghoachani, Electrical, thermal and optical modeling of photovoltaic systems: Step-by-step guide and comparative review study, Sustainable Energy Technol. Assess. 49 (2022) 101711, https://doi.org/10.1016/J.SETA.2021.101711.
[12] Gu, W., Ma, T., Ahmed, S., Zhang, Y., & Peng, J. (2020). A comprehensive review and outlook of bifacial photovoltaic (bPV) technology. In Energy Conversion and Management (Vol. 223, p. 113283). Elsevier Ltd. https://doi.org/10.1016/j.enconman.2020.113283.
[13] W. Gu, T. Ma, M. Li, L. Shen, Y. Zhang, A coupled optical-electrical-thermal model of the bifacial photovoltaic module, Appl. Energy 258 (October 2019) (2020) 114075, https://doi.org/10.1016/j.apenergy.2019.114075.
[14] *IEC* 61724-1:2021, "Photovoltaic system performance, Part 1: Monitoring." (2021).
[15] IRENA Renewable Cost Database. (2020). Renewable Power Generation Costs in 2020. In International Renewable Energy Agency.
[16] K. Ishaque, Z. Salam, An improved modeling method to determine the model parameters of photovoltaic (PV) modules using differential evolution (DE), Sol. Energy 85 (9) (2011) 2349–2359, https://doi.org/10.1016/j.solener.2011.06.025.
[17] ITPRV. (2022). International Technology Roadmap for Photovoltaic. Results 2021 including maturity report 2022. In Itrpv: Vol. 13th Editi (Issue Thirteenth Edition, November 2022). https://itrpv.vdma.org/en/ueber-uns.
[18] T. Katsaounis, K. Kotsovos, I. Gereige, A. Basaheeh, M. Abdullah, A. Khayat, E. Al-Habshi, A. Al-Saggaf, A.E. Tzavaras, Performance assessment of bifacial c-Si PV modules through device simulations and outdoor measurements, Renew. Energy 143 (2019) 1285–1298, https://doi.org/10.1016/j.renene.2019.05.057.
[19] O.A. Katsikogiannis, H. Ziar, O. Isabella, Integration of bifacial photovoltaics in agrivoltaic systems: A synergistic design approach, Appl. Energy 309 (July 2021) (2022) 118475, https://doi.org/10.1016/j.apenergy.2021.118475.
[20] T. Khatib, W. Elmenreich, Modeling of photovoltaic systems using Matlab: Simplified green codes, John Wiley & Sons, 2016.
[21] King, D. L., Boyson, W. E., & Kratochvil, J. A. (2004). Photovoltaic array performance model. Sandia Report No. 2004-3535, 8, 1–19. https://doi.org/10.2172/919131.
[22] J.R. Ledesma, R.H. Almeida, F. Martinez-Moreno, C. Rossa, J. Martín-Rueda, L. Narvarte, E. Lorenzo, A simulation model of the irradiation and energy yield of large bifacial photovoltaic plants, Sol. Energy 206 (August 2019) (2020) 522–538, https://doi.org/10.1016/j.solener.2020.05.108.
[23] Mannino, G., Tina, G. M., Cacciato, M., Todaro, L., & Bizzarri, F. (2022). Experimental assessment of temperature estimation models of bifacial photovoltaic modules. 7, 214–216. https://doi.org/10.1109/PVSC48317.2022.9938792.
[24] Mathworks, C. (2022). Curve Fitting Toolbox ™ User ' s Guide R 2022 b.
[25] M.J. Mayer, G. Gróf, Extensive comparison of physical models for photovoltaic power forecasting, Appl. Energy 283 (December 2020) (2021), https://doi.org/10.1016/j.apenergy.2020.116239.
[26] E.I. Ortiz-Rivera, F.Z. Peng, Analytical model for a photovoltaic module using the electrical characteristics provided by the manufacturer data sheet, PESC Record - IEEE Annual Power Electronics Specialists Conference 2005 (2005) 2087–2091, https://doi.org/10.1109/PESC.2005.1581920.
[27] Phimu, K., Singh, K. J., & Sankar Dhar, R. (2021). Novel SPICE Model for bifacial solar cell to increase the renewable power generation. Proceedings of 4th International Conference on 2021 Devices for Integrated Circuit, DevIC 2021, 129–133. https://doi.org/10.1109/DevIC50843.2021.9455939.
[28] N. Riedel-lyngskær, D. Berrian, D.A. Mira, A.A. Protti, P.B. Poulsen, J. Libal, J. Vedde, Validation of bifacial photovoltaic simulation software against monitoring data from large-scale single-axis trackers and fixed tilt systems in Denmark, Appl. Sci. (Switzerland) 10 (23) (2020) 1–29, https://doi.org/10.3390/app10238487.
[29] E. Saloux, A. Teyssedou, M. Sorin, Explicit model of photovoltaic panels to determine voltages and currents at the maximum power point, Sol. Energy 85 (5) (2011) 713–722, https://doi.org/10.1016/j.solener.2010.12.022.
[30] I. Shoukry, J. Libal, R. Kopecek, E. Wefringhaus, J. Werner, Modelling of Bifacial Gain for Stand-alone and in-field Installed Bifacial PV Modules, Energy Procedia 92 (2016) 600–608, https://doi.org/10.1016/j.egypro.2016.07.025.
[31] E. Skoplaki, J.A. Palyvos, On the temperature dependence of photovoltaic module electrical performance: A review of efficiency/power correlations, Sol. Energy 83 (5) (2009) 614–624, https://doi.org/10.1016/j.solener.2008.10.008.
[32] Smith, B. L., Woodhouse, M., Horowitz, K. A. W., Silverman, T. J., Zuboy, J., Margolis, R. M., Smith, B. L., Woodhouse, M., Horowitz, K. A. W., Silverman, T. J., Zuboy, J., & Margolis, R. M. (2021). Photovoltaic (PV) Module Technologies: 2020 Benchmark Costs and Technology Evolution Framework Results Photovoltaic (PV) Module Technologies : 2020 Benchmark Costs and Technology Evolution Framework Results. November.
[33] Stein, J. S., Reise, C., Castro, J. B., Friesen, G., Maugeri, G., Urrejola, E., & Ranta, S. (2021). Bifacial PV modules & systems Experience and Results from International Research and Pilot Applications. In IEA, International Energy Agency. https://iea-pvps.org/wp-content/uploads/2021/04/IEA-PVPS-T13-14_2021-Bifacial-Photovoltaic-Modules-and-Systems-report.pdf.
[34] X. Sun, M.R. Khan, C. Deline, M.A. Alam, Optimization and performance of bifacial solar modules: A global perspective, Appl. Energy 212 (December 2017) (2018) 1601–1610, https://doi.org/10.1016/j.apenergy.2017.12.041.
[35] B. Taghezouit, F. Harrou, C. Larbes, Y. Sun, S. Semaoui, A.H. Arab, S. Bouchakour, Intelligent monitoring of photovoltaic systems via simplicial empirical models and performance loss rate evaluation under LabVIEW: A case study, Energies 15 (21) (2022) 7955, https://doi.org/10.3390/en15217955.
[36] B. Taghezouit, F. Harrou, Y. Sun, A.H. Arab, C. Larbes, A simple and effective detection strategy using double exponential scheme for photovoltaic systems monitoring, Sol. Energy 214 (May) (2021) 337–354, https://doi.org/10.1016/j.solener.2020.10.086.
[37] H. Tian, F. Mancilla-David, K. Ellis, E. Muljadi, P. Jenkins, A cell-to-module-to-array detailed model for photovoltaic panels, Sol. Energy 86 (9) (2012) 2695–2706, https://doi.org/10.1016/j.solener.2012.06.004.
[38] G.M. Tina, C. Ventura, S. Ferlito, S. De Vito, A state-of-art-review on machine-learning based methods for PV, Applied Sciences (switzerland) 11 (16) (2021), https://doi.org/10.3390/app11167550.
[39] A.K. Tossa, Y.M. Soro, Y. Azoumah, D. Yamegueu, A new approach to estimate the performance and energy productivity of photovoltaic modules in real operating conditions, Sol. Energy 110 (2014) 543–560, https://doi.org/10.1016/j.solener.2014.09.043.
[40] M.G. Villalva, J.R. Gazoli, E.R. Filho, Comprehensive approach to modeling and simulation of photovoltaic arrays, IEEE Trans. Power Electron. 24 (5) (2009) 1198–1208, https://doi.org/10.1109/TPEL.2009.2013862.
[41] Villalva, M. G., Gazoli, J. R., & Ruppert Filho, E. (2009). Modeling and circuit-based simulation of photovoltaic arrays. 2009 Brazilian Power Electronics Conference, COBEP2009, 1244–1254. https://doi.org/10.1109/COBEP.2009.5347680.
[42] Vogt, M. R., & Pilis, G. (2023). Developing an energy rating for bifacial photovoltaic modules. August 2022, 1–12. https://doi.org/10.1002/pip.3678.
[43] H. Ziar, F.F. Sönmez, O. Isabella, M. Zeman, A comprehensive albedo model for solar energy applications: Geometric spectral albedo, Appl. Energy 255 (2019) 113867, https://doi.org/10.1016/J.APENERGY.2019.113867.